FINITE ELEMENT ANALYSIS OF WELDING RESIDUAL STRESS OF ALUMINUM PLATES UNDER DIFFERENT BUTT JOINT PARAMETERS

G. Mi[1] – C. Li[1] – Z. Gao[1*]– D. Zhao[1] – J. Niu[1]

[1]School of Materials Science and Engineering, Henan Polytechnic University, Henan, Jiaozuo, 454003, P. R. China

ARTICLE INFO

***Article history*:**
Received: 09.07.2013.
Received in revised form: 18.09.2013.
Accepted: 26.9.2013.

Keywords:
Heat source model
Residual stress
Finite element
Thermal-elastoplastic

Abstract:

A thermal-elastoplastic finite element method was built to simulate the process of variable polarity plasma arc welding (VPPAW) for aluminum alloy plates. The welding temperature and stress fields of the aluminum plates with different butt joint parameters (intervals of the joints: D=0.3 mm, 2 mm; unfitness of the joints: L=0.3 mm, 2 mm) were calculated using a 3D double-ellipsoidal heat source model. The residual stresses of the welded plates were predicted; the results showed that the unfitness of the joint has a greater impact on the welding residual stresses than that of the interval. The simulated and experimental results were compared and they showed that they are well consistent with each other.

1 Introduction

Aluminum alloys are important lightweight structural materials that have been widely used in aviation, aerospace, transportation and other areas for their excellent specific strength and good weldability [1]. In recent years, the applications of aluminum alloy sheets and their welded structures have drawn more and more attention because of their light weight and ease of processing. However, due to rapid local heating, the distribution of internal temperature in the weldment is uneven. This, together with their larger thermal conductivity and lower high-temperature strength often lead to greater residual stress and deformation of the welded components, which can result in a series of issues such as low intensity, instability of the joint in size and small ductile deformation, limiting thus their further development and applications. In addition, different welding methods and welded structures will produce different types of welding residual stress, which also brings a challenge to the assessment of the stability and reliability of the welded structures. With the development of numerical simulation technology, understanding of welding residual stress and deformation has not been dependent solely on the physical measurements; it can be also predicted using finite element simulation methods quickly and accurately [2-6]. At present, the vast majorities of research on the welding numerical simulations are reported to be aiming at TIG or MIG welding, but less at the plasma arc welding (PAW), particularly at variable polarity plasma arc welding (VPPAW). In this paper, the VPPAW process of aluminum alloy plates was numerically simulated by using finite element software, and the residual stress after welding was predicted. Finally, the final finite element calculation results of the residual stress were compared with experimental results to verify the applicability of the finite element simulation.

[*] Corresponding author. Tel.: 0086-13839134383; fax: 0086-391-3986901
E-mail address: mrgaozeng@163.com

2 Experimental materials and testing methods

Two LF6 aluminum alloy plates with a thickness of 5 mm, and 150 mm×75 mm (Length × Width), were prepared for welding. The nominal chemical composition of this alloy is presented in Table 1.

Table 1. Chemical composition of LF6 aluminum alloy (wt.%).

Element	Mg	Mn	Ti	Fe
wt.%	5.8~6.8	0.5~0.8	0.02~0.1	≤0.4
Element	Si	Zn	Cu	Al
wt.%	≤0.4	≤0.2	0.1	Balance

The surfaces of the samples were chemically cleaned with acetone to eliminate any surface contamination before welding. The samples were placed flat on top of a platform prior to welding.

There are four kinds of intervals (see Fig. 1 and Fig. 2) between the two plates: 0.3 mm, and 2 mm for butt joint: 0.3 mm, and 2 mm for unfitness butt joint. LF6 aluminum alloy wire was used as a filler metal. The shielding gas is pure argon, and the welding power is alternating current (AC). The standard welding conditions used for these welds are listed in Table 2.

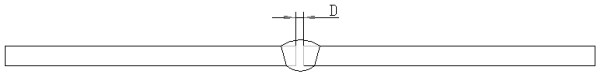

Figure 1. A schematic drawing of the butt joint (D= 0.3mm; 2mm).

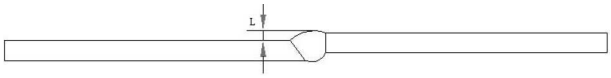

Figure 2. A schematic drawing of the unfitness butt joint (L= 0.3mm; 2mm).

Table 2. Standard welding conditions used for this program

Plasma gas	DCEN current	DCEP current	DCEN time	DCEN time	Welding speed
2.0L/min	130A	2.5mm	21ms	4ms	0.18m/min

Table 3. Material property parameters

Temperature ℃	Elastic ratio GPa	Yield Strength MPa	Thermal conductivity W /(m• ℃)	Specific heat J/(kg • ℃)	Linear expansion coefficient 10^{-6} • $℃^{-1}$
20	70.0	300	117	900	22.8
100	60.8	280	121	921	23.1
200	54.4	240	126	1005	24.7
300	43.1	160	130	1047	25.5
400	32.0	113	138	1089	26.5

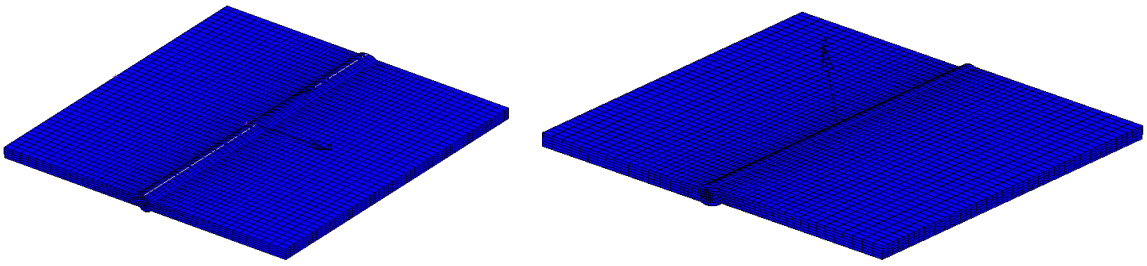

Figure 3. Mesh of the model: (a) internal of butt joint D =2 mm; (b) unfitness of butt joint L= 2 mm.

3 Finite element model

3.1 Model mesh [7]

The finite element model was established on a scale of 1:1. Due to a great temperature drop from the weld to its surrounding area, finer grids were used in the former, while coarse grids were adopted in the latter; in other words, the overall performance of the transition is from dense to sparse. This approach of meshing division can not only ensure accuracy of the calculation, but also reduce the computing time. The finite element model geometry is divided into 15200 eight-node hexahedral elements and 18717 nodes, as shown in Fig. 3.

3.2 Thermal physical parameters

The material property parameters include mechanical properties and thermal physical parameters, which are functions of temperature. In the simulation, a piece-wise linearization form of 'temperature-corresponding performance' was established to provide computer program and was assigned to units as material properties, as shown in Table 3, in which the yield strength was obtained by high-temperature tensile test.

3.3 The heat source model and boundary conditions

Welding residual stress and deformation are produced due to the heterogeneous temperature field caused by localized heat input in the welding process. In the VPPAW welding process, beam-plasma is taken as the heat source to heat the metal surface, in which the main mode of heat conduction is heat transfer.

The heat conduction equation is as follows:

$$\rho c\frac{\partial T}{\partial t}=\frac{\partial}{\partial x}(k\frac{\partial T}{\partial x})+\frac{\partial}{\partial y}(k\frac{\partial T}{\partial y})+\frac{\partial}{\partial z}(k\frac{\partial T}{\partial z})+Q \quad (1)$$

Where ρ is density, c is the specific heat capacity, k is the thermal conductivity coefficient, and Q is the heat flux.

In the numerical calculation process, a three-dimensional double ellipsoid heat source model (as shown in Fig. 4) is taken as the heat source model [8]. The model equations are as follows.

The heat source expression of the first half of the ellipsoid:

$$q(x,y,z,t)=\frac{6\sqrt{3}Qf_f}{abc_1\pi\sqrt{\pi}}e^{-3(\frac{x^2}{a^2}+\frac{y^2}{b^2}+\frac{(z-vt)^2}{c_1^2})} \quad (2)$$

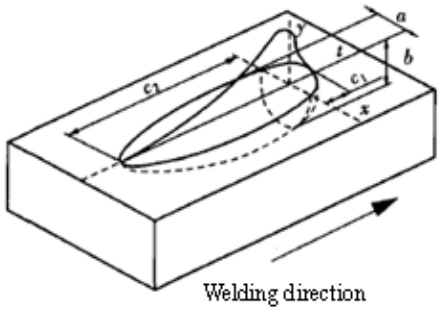

Figure 4. 3D-double ellipsoid head source model.

The heat source expression of the second half of the ellipsoid

$$q(x,y,z,t)=\frac{6\sqrt{3}Qf_r}{abc_2\pi\sqrt{\pi}}e^{-3(\frac{x^2}{a^2}+\frac{y^2}{b^2}+\frac{(z-vt)^2}{c_2^2})} \quad (3)$$

In Eq. (2) and Eq. (3): a is the half axle in y direction of the ellipsoid (mm), b is the half axle in the z direction of the ellipsoid (mm), c_1 is the first half axle in the x direction of the *ellipsoid (mm)*, c_2 is the second half axle in the x direction of the ellipsoid *(mm)*, Q is the total heat power, and $Q = \eta IU$, where η is the thermal efficiency of the welding heat source, v is welding speed, *ff* and *fr* are respectively on behalf of the energy fraction of the heat source pre and post of the ellipsoid so that $f_f + f_r = 2$. In accordance with the test specification and the measurement of the weld, η=0.7, a=6 mm, b=7 mm, c_1= 7 mm, c_1= 3 mm, and c_2=7 mm.

The boundary conditions of a finite element model include thermal boundary conditions and mechanical constraint boundary conditions, in which the main consideration of the thermal boundary conditions is heat radiation, heat conduction and convection thermal cooling. The main consideration of the mechanical boundary conditions is to simulate the constraints of the fixtures on the workpiece during the welding process and the constraints of removing the fixture after cooling to room temperature [9].

4 The simulation results of welding residual stress

4.1 Welding temperature field

Figure 5 shows the transient temperature field distribution cloud of the welds at the welding time of t = 39 s. Figure 6 shows the residual stress distribution cloud of the weldment after welding is completed (taking the 0.3 mm gap for example).

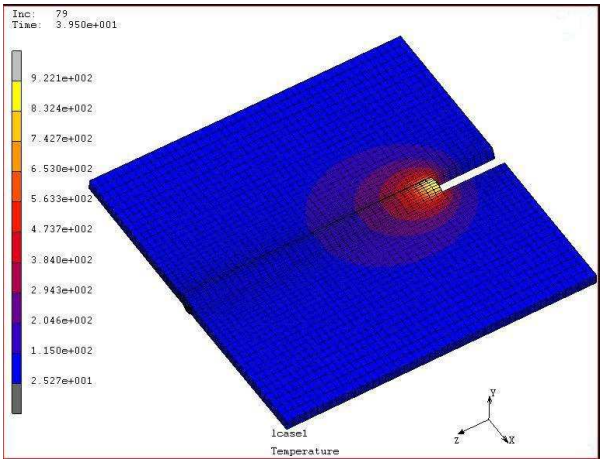

Figure 5. Welding temperature field; t =39s.

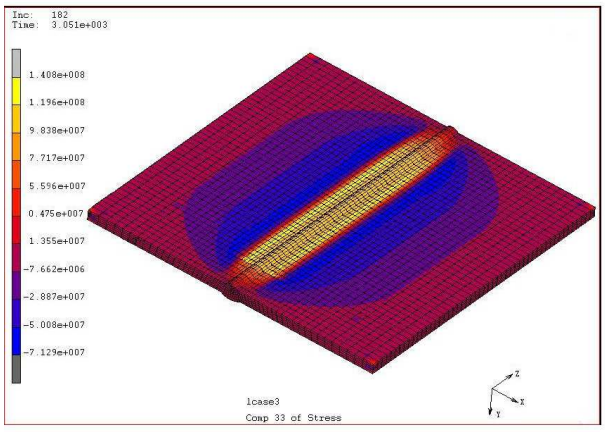

Figure 6. Residual stress field; t =3000s.

It can be seen from Fig. 5 that in the welding process, a dramatic temperature change occurs between the weld and the surrounding area, in which the maximum temperature lies in the weld area where a temperature above 900°C can be achieved. In addition, the temperature gradient is decreased by increasing distance from the weld, while the temperature difference at the different positions will inevitably lead to the regional stress variations. From the residual stress field of the weldment shown in Fig. 6, we can see that high stress exists in the vicinity of the weld and the heat affected zone.

4.2 Welding residual stress

Figure 7 shows the longitudinal residual stress curves of the specimen welded and cooled to room temperature; the four different forms are: butt joint gap of 0.3 mm and 2 mm; and unfitness butt joint gap of 0.3 mm and 2 mm.

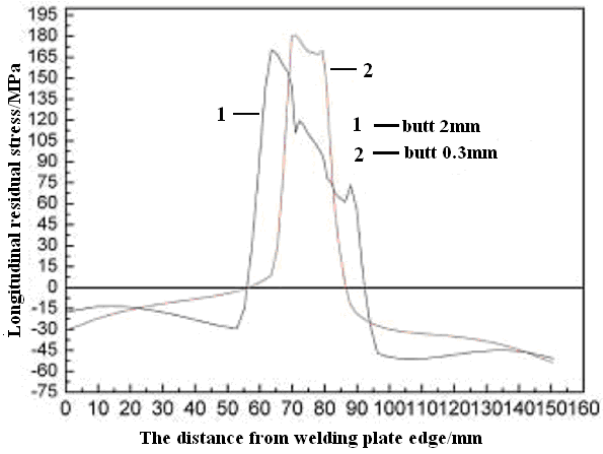

(a)

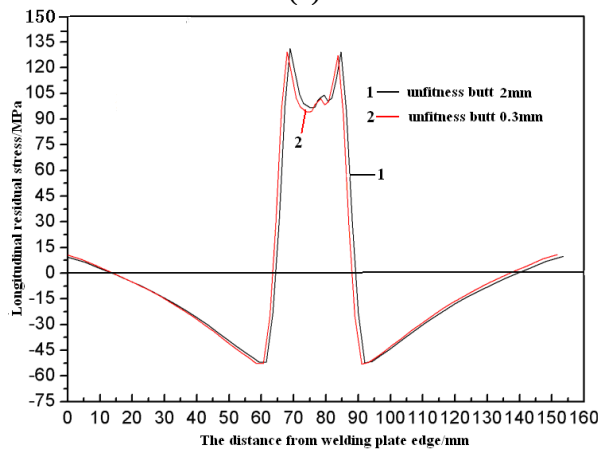

(b)

Figure 7. Curves of welding longitudinal residual stress (a) unfitness type; (b) internal type.

Figure 7 shows that the residual stress curve representing the butt welding parts of the aluminum alloy plates was symmetrical along the seam, and the one representing weldments with 0.3 mm and 2 mm gap butt joints did not change significantly.

But for unfitness of butt joint weldments/unfitness of welded but joints, the residual stress is significantly different in size and in the regional distribution along both sides of the weld, and the maximum residual stress lies in one side of the weld. The maximum residual stress of the weldments with 0.3 mm unfitness is higher than that of the weldment with 2 mm unfitness.

5 Welding procedure and results

5.1 Measurement of welding residual stress [10-12]

In order to verify the accuracy of the finite element model calculations, an experimental determination of the residual stress for the plates after welding has been carried out. Amongst the welding residual stress measurement methods, the hole-drilling method is proved to be convenient and accurate. Therefore, the longitudinal residual stress of the specimen was tested after welding by using the hole drilling method. The location of strain gauges is shown in Fig. 8, and the measurement results were compared with the finite element simulations.

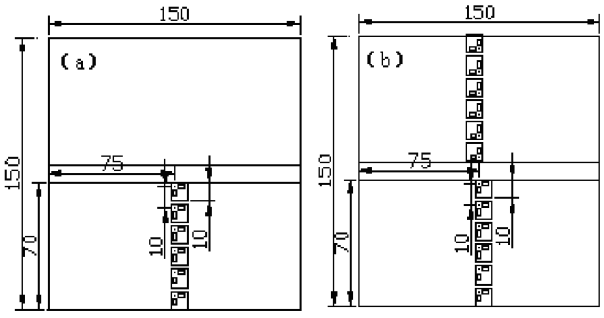

Figure 8. The location of the strain gauges (a) butt type; (b) unfitness butt type.

5.2 Comparison of measured value and calculated value

We can see from Fig. 9 that the simulation results and the test results were in good agreement, which thus verifies the finite element model and approves its accuracy and applicability.

6 Conclusions

A significant difference of welding residual stress exists in the aluminum alloy plate VPPAW butt

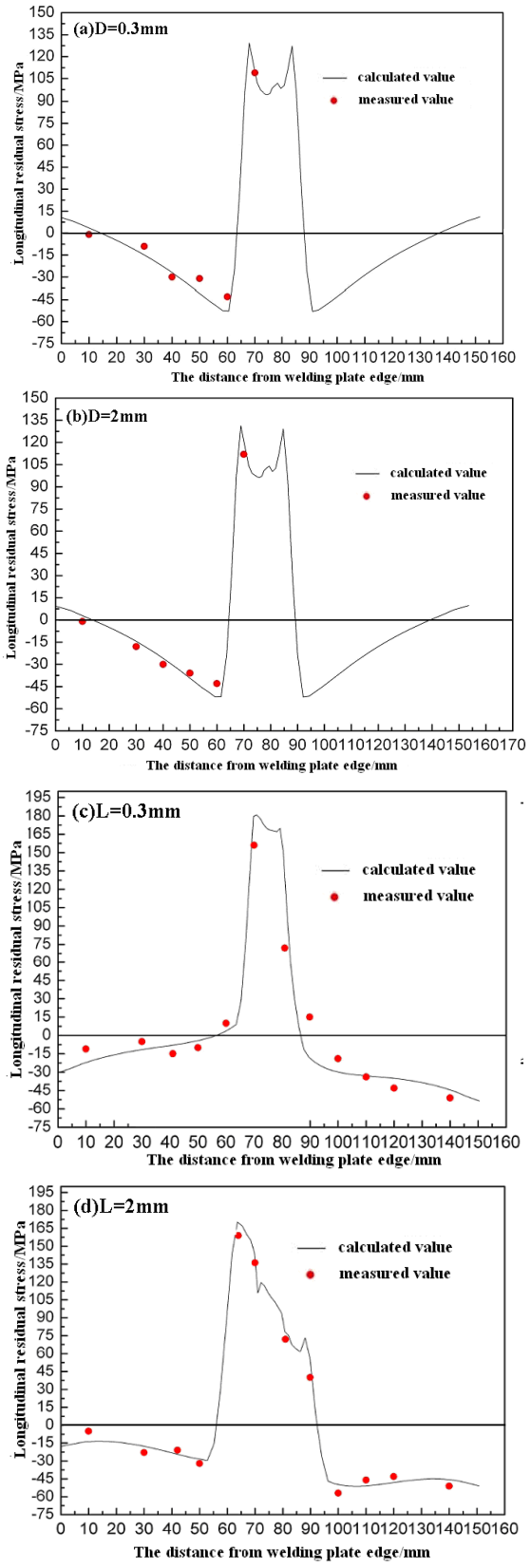

Figure 9. Comparison of the actual measurement and the calculation results of the welding residual stress.

joints with different parameters. The effect of a gap type of the butt joint on the residual stress is less significant than that of the unfitness of a butt joint. The residual stress change is not significant in butt joint weldments with a gap of 2 mm or 0.3 mm, while it is obvious in unfitness of butt joint weldments with the same gap sizes. The highest value of residual stress for the unfitness of butt joint welded part with a gap of 0.3 mm is higher than that of the butt joint with a 2 mm joint. The residual stress determinated by the hole-drilling method has good agreement with the simulation results, which indicates that the three-dimensional double ellipsoid heat source model and the thermal boundary conditions are appropriate in simulating the thermal process of the aluminum alloy Plate VPPAW welding. Undoubtedly, the reliability of simulation results is very high.

Acknowledgement

Space environment service performance evaluation of aluminum alloy welded joints (National Natural Science Foundation funded project: 90,205,035)

References

[1] Jones, B.K., Emery, A.F., Marburger, S.I.: *An analytical and experimental study of the effects of welding parameters on fusion welds*, Welding Journal 72 (1993), 51-59.

[2] Rokhlin, S.I., Guu, A.C.: *A Study of arc force, pool depression and weld penetration during gas tungsten arc welding*, Welding Journal 72 (1993), 381-390.

[3] Brown, S.B., Song, H.: *Implications of three dimensional numerical simulations of welding of large structures*, Welding Journal 71 (1992), 55-56.

[4] Teng, T.L., Chang, P.H., Ko, H. CH.: *Finite element analysis of circular patch welds*, International Journal of Pressure Vessels and Piping 77 (2000), 643-650.

[5] Sabapathy, P.N., Wahab, M.A., Painter, M.J., *Numerical models of in-service welding of gas pipelines*, Journal of Materials Processing Technology 118 (2001), 14–21.

[6] Klobčar, D., Tušek, J., Taljat, B.: *Finite element modeling of GTA weld surfacing applied to hot-work tooling*, Computational Materials Science 31 (2004), 368-378.

[7] Wu, C.S.: *Welding Thermal Process of Numerical Analysis*, Harbin Institute of Technology Press, Harbin, 1990.

[8] Xue, Z.M., Gu, L., Zhang, Y.H.: *Laser welding temperature field, numerical simulation*, Welding Journal 24 (2003), 79-82

[9] Goldak, J., Bibby, M., Downey, D., Gu, M., *Heat and fluid flow in welds*, International Institute of Welding Congress on Joining Research, Advanced Joining Technologies, Chapman and Hall, 1990, 69–82.

[10] Fricke, S., Keim, E., Schmidt, J.: *Numerical weld modeling—a method for calculating weld-induced residual stresses*, Nuclear Engineering and Design 206 (2001), 139-150.

[11] Liu, B.L., Jiao J. Q., Lu D.: *Determination of welding residual stress hole when the plastic to release strain*, Dalian Railway Institute 15 (1994), 87-94.

[12] Chen, Y., Gao, D.P., Chen, X.: *Titanium plate electron beam welding residual stress measurement of the hole*, Physical and Chemical Tests-Physical 37 (2001), 427-430.